Manwaring, W. H. (1910) *Z. Immunitaetsforsch. 6*, 513.
Marsh, D., Watts, A., & Knowles, P. F. (1976) *Biochemistry 15*, 3570.
Martin, F. J., & McDonald, R. C. (1976) *Biochemistry 15*, 321.
Mitaku, S., Ikegami, A., & Sakanishi, A. (1978) *Biophys. Chem. 8*, 295.
Mulder, E., de Gier, I., & van Deenen, L. L. M. (1963) *Biochim. Biophys. Acta 20*, 94.
Munder, P. G., Modolell, M., Raetz, W., & Luckenbach, G. A. (1973) *Eur. J. Immunol. 3*, 454.
Nagle, J. F., & Scott, H. L. (1978) *Biochim. Biophys. Acta 513*, 236.
Papahadjopoulos, D., Jacobson, K., Nir, S., & Isac, T. (1973) *Biochim. Biophys. Acta 311*, 330.
Papahadjopoulos, D., Nui, S., Vail, W. I., & Poste, G. (1976) *Biochim. Biophys. Acta 448*, 245.
Phillips, M. C., Graham, D. E., & Hauser, H. (1975) *Nature (London) 254*, 154.
Poole, A. R., Howell, J. I., & Lucy, J. A. (1970) *Nature (London) 227*, 810.
Poste, G., & Allison, A. C. (1973) *Biochim. Biophys. Acta 300*, 421.
Reman, R. C., Demel, R. A., de Gier, J., van Deenen, L. L. M., Eibl, H., & Westphal, D. (1969) *Chem. Phys. Lipids 3*, 221.
Robertson, A. F., & Lands, W. E. M. (1964) *J. Lipid Res. 5*, 88.
Smoluchowski, M. (1917) *Z. Phys. Chem., Stoechiom. Verwandtschaftsl. 92*, 129.
Thomas, J. K., Grieser, F., & Wong, M. (1977) *Ber. Bunsenges. Phys. Chem. 82*, 937.
Tsong, T. Y. (1975) *Biochemistry 14*, 5409.
van Deenen, L. L. M. (1965) *Prog. Chem. Fats Other Lipids 8* (*Part* 1), 17-33.
van Echteld, C. J. A., de Kruijff, B., & de Gier, J. (1980) *Biochim. Biophys. Acta 595*, 71.
von Dreele, P. H. (1978) *Biochemistry 17*, 3939.
Weltzien, H. U. (1979) *Biochim. Biophys. Acta 559*, 259.
Woolley, P., & Diebler, H. (1979) *Biophys. Chem. 10*, 305.
Wu, S., & McConnell, H. M. (1973) *Biochem. Biophys. Res. Commun. 55*, 484.

Structure and Dynamics of Phospholipid Membranes: An Electron Spin Resonance Study Employing Biradical Probes†

Peter Meier, Alfred Blume, Ernst Ohmes, Franz A. Neugebauer,‡ and Gerd Kothe*

ABSTRACT: The large zero-field splitting of rigid biradicals makes them important candidates for spin probes of phospholipid membranes. Here we develop an electron spin resonance line-shape model for such probes on the basis of the stochastic Liouville equation. Particular emphasis is given to the slow-diffusional regime, characteristic of bilayers in the gel phase. The theory is employed to study the line shapes of bis(verdazyl) biradicals, incorporated into oriented multibilayers of dimyristoylphosphatidylcholine. Computer simulations of the *angular-dependent spectra* provide the orientational distribution functions and rotational correlation times of the spin probes. They occupy two different sites in bilayer membrane. The orientational distribution of the spin probes is related to the structure of the phospholipid phases. In the $L_{\beta'}$ phase the hydrocarbon chains are uniformly tilted by $\delta = 23°$ with respect to the bilayer normal. For the $P_{\beta'}$ phase we observe a random distribution of tilt angles from $\delta = 0°$ to $\delta = 19°$, indicating that the chains orient perpendicular to the local (rippled) bilayer surface. This structure has not been established previously. In agreement with other studies we find no tilt for the L_α phase. The order parameters of the hydrocarbon chains increase with decreasing temperature, jumping from $S \leq 0.6$ to $S \geq 0.8$ at the main transition. From the rotational correlation times of the spin probes, intrinsic bilayer viscosities of $0.08\ P \leq \eta \leq 20\ P$ ($50\ °C \geq T \geq 1\ °C$) are determined. An Arrhenius plot provides activation energies of the viscous flow. The values increase from $E_{visc} \sim 10$ kcal/mol in the L_α phase to $E_{visc} \sim 18$ kcal/mol in the $L_{\beta'}$ phase.

The present knowledge about the physical properties of biological membranes originates to a great extent from studies of model membranes, prepared from natural and synthetic phospholipids. Fully hydrated phosphatidylcholines form bilayer structures, which exist in two distinctly different phases. The nature of the liquid-crystalline phase has been well characterized by different techniques [for a recent review, see Grell (1981)]. The detailed organization of the bilayer in the gel phase is less clearly understood. Particularly, the nature of an endothermic event, generally referred to as the pretransition, is still the subject of discussion.

In the present study we investigate this problem with electron spin resonance spectroscopy (ESR),[1] using rigid biradicals as spin probes. They possess one clear advantage over their monoradical counterparts; for in addition to the Zeeman and hyperfine interaction, there is also the totally anisotropic

† From the Institute of Physical Chemistry, University of Freiburg, D-7800 Freiburg, Federal Republic of Germany. *Received April 2, 1981.* This work was supported by Deutsche Forschungsgemeinschaft and Fonds der Chemischen Industrie.

‡ Present address: Max-Planck-Institut für Medizinische Forschung, Abteilung Organische Chemie, D-6900 Heidelberg, Federal Republic of Germany.

[1] Abbreviations: ESR, electron spin resonance; BVL, 3,3′-(1,4-phenylene)bis(verdazyl); DMPC, dimyristoylphosphatidylcholine; NMR, nuclear magnetic resonance; DPH, 1,6-diphenyl-1,3,5-hexatriene; STESR, saturation transfer electron spin resonance.

0006-2960/82/0421-0526$01.25/0

zero-field splitting. Unlike the other two, its magnitude varies drastically with the structure of the biradical (Kothe & Wilker, 1980; Forrester, 1980). Since the correlation times that can be determined by spin probe techniques depend on the anisotropy of the magnetic interaction, rigid biradicals are more sensitive to molecular motions than the corresponding monoradicals (Kothe et al., 1978). Moreover the larger anisotropy also facilitates studies involving molecular structure and ordering (Keana & Dinerstein, 1971). However, due to the lack of a comprehensive line-shape model, quantitative investigations are rare [for a review, see Luckhurst (1976)]. In this paper we first develop the theory necessary to understand the ESR spectra of biradical spin probes in membranes. Particular emphasis is given to the slow-diffusional regime, characteristic of bilayers in the gel phase. Molecular order is considered by a comprehensive distribution function, in which director and magnetic field may have arbitrary orientations.

The theory is then applied to the analysis of temperature and *angular-dependent ESR spectra* of bis(verdazyl) radicals (BVL), incorporated into oriented multibilayers of dimyristoylphosphatidylcholine (DMPC). Computer simulations provide the orientational distribution functions and rotational correlation times of the spin probes. They are related to molecular order and dynamics of the bilayer membrane.

The orientational distributions of the biradicals sensitively reflect the structure of the phospholipid phases. Detailed information about the organization of the hydrocarbon chains is obtained. From the rotational correlation times intrinsic viscosities are determined. The results, referring to both phases, are discussed in relation to other studies of the dynamic properties of membranes.

Theory

In this section we briefly develop an ESR line-shape model for biradical spin probes in membranes with particular reference to the slow-motional region, where the conventional Redfield theory (Redfield, 1965) no longer applies. Generally, the absorption line shape $L(\omega)$ for an ensemble of radicals is given by

$$L(\omega) = \mathrm{Im}\,[\mathrm{Tr}\,(\rho \cdot \mathbf{S}_+)\exp(-i\omega t)] \tag{1}$$

where $\mathbf{S}_+$ is the raising operator, ω is the angular frequency of the microwave field, and ρ is the spin density matrix, assumed to obey the stochastic Liouville equation (Kubo, 1969; Norris & Weissman, 1969; Freed et al., 1971; Kothe, 1977):

$$\dot{\rho}_{AB} = (i/\hbar)\,[\rho_{AB}, \mathcal{H}_{AB}] + (\dot{\rho}_{AB})_{relax} + (\dot{\rho}_{AB})_{rotdif}$$

$$(\dot{\rho}_{AB})_{rotdif} = \sum_{A'} (\mathbf{k}_{A'ABB'} \cdot \rho_{A'B} - \mathbf{k}_{AA'BB'} \cdot \rho_{AB}) + \sum_{B'} (\mathbf{k}_{AABB'} \cdot \rho_{AB'} - \mathbf{k}_{AABB'} \cdot \rho_{AB}) \tag{2}$$

Here $\mathcal{H}_{AB}$ is the spin Hamiltonian of the radical, $(\dot{\rho}_{AB})_{relax}$ is a phenomenological relaxation term, and $(\dot{\rho}_{AB})_{rotdif}$ is to account for the spin diffusion caused by the rotational motion of the radical. It is assumed that only a finite number of angular positions or sites, denoted by the index AB, can be occupied during this process. Each site is characterized by a set of Euler angles (θ_A and ϕ_B), relating the diffusion tensor system **X**, **Y**, and **Z** to the laboratory system **x**, **y**, and **z**, which we choose with the z axis parallel to the static magnetic field (see Figure 1).

The matrices $\mathbf{k}_{AA'BB}$ in eq 2 are multiples of the unit matrix, characterizing the rate at which radicals at site AB move into site A'B. The values for the transition rates depend upon the model used to describe the rotational motion. In the case of Brownian diffusion (reorientation through a sequence of infinitesimally small angular steps), the transition rates must satisfy the following equations (Kothe et al., 1979):

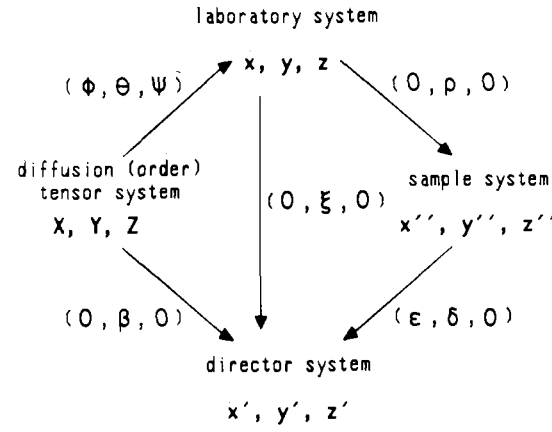

FIGURE 1: Notation for coordinate systems and Euler transformations, used in the ESR line-shape model. The definition of the Euler angles corresponds to that of Van et al. (1974).

$$k_{AA+1BB} + k_{AA-1BB} = N_\theta^2/(3\pi^2\tau_\perp)$$

$$k_{AABB+1} + k_{AABB-1} = N_\phi^2/(12\pi^2\tau_\parallel)$$

$$k_{AA'BB} n_{AB} = k_{A'ABB} n_{A'B}$$

$$k_{AABB'} n_{AB} = k_{AAB'B} n_{AB'} \tag{3}$$

where N_θ and N_ϕ are the number of sites, chosen to mimic a continuous distribution of the radicals. Solving eq 3, one can establish values for all transition rates in terms of two rotational correlation times, $\tau_\perp$ and $\tau_\parallel$, and the equilibrium populations, n_{AB}, of the sites. $\tau_\perp$ is the correlation time for reorientation of the symmetry axis of the diffusion tensor, while $\tau_\parallel$ refers to rotation about it.

The number of radicals, n_{AB}, in a particular site is related to the normalized orientational distribution function

$$f(\phi,\theta,\psi) = N_1 \exp[C(\cos\theta\cos\xi - \sin\theta\cos\psi\sin\xi)^2] \tag{4}$$

by an integration over the area of that site. In deriving eq 4 from statistical theories of nematic liquid crystals (Maier & Saupe, 1959; Cotter, 1977), we assumed that the order tensor is axially symmetric in **X**, **Y**, and **Z**. The coefficient C in eq 4 characterizes the orientation of the radicals with respect to a local director **z'**, while the angle ξ specifies the orientation of **z'** in the laboratory frame (see Figure 1). In unoriented membrane systems, such as vesicles or liposomes, the director axes are randomly distributed. In macroscopically ordered bilayers, however, **z'** can be specified with respect to a sample system **x''**, **y''**, and **z''**, generally defined by the glass plate, used to prepare the sample. If ρ denotes the angle between **z''** (glass plate normal) and **z**, $\cos\xi$ is found to be

$$\cos\xi = \cos\delta\cos\rho - \sin\delta\cos\epsilon\sin\rho \tag{5}$$

where ϵ and δ are the polar coordinates of the director in the sample system (see Figure 1). Of course, all director axes need not to have the same orientation; instead they may be distributed according to the probability function

$$f(\epsilon,\delta) = N_2 \quad \text{if } \delta_{min} \le \delta \le \delta_{max}$$
$$= 0 \quad \text{otherwise} \tag{6}$$

where N_2 is a normalization constant. The angles ϵ and δ are the varied, and each spectrum for a given set of angles is weighted by eq 6.

The spin Hamiltonian for a biradical, exhibiting Zeeman, exchange, dipolar, and hyperfine interactions, may be written as (Reitz & Weissman, 1960; Luckhurst, 1976)

$$\mathcal{H} = g_{zz}\mu_B B_z S_z + J\mathbf{S}^{(1)}\cdot\mathbf{S}^{(2)} + \tfrac{3}{2}D_{zz}(S_z^2 - \tfrac{1}{3}S^2) + A_{zz}(S_z^{(1)}I_z^{(1)} + S_z^{(2)}I_z^{(2)}) + \mathcal{H}_{\text{p-sec}} + \mathcal{H}_{\text{n-sec}} + \mathcal{H}_{\text{rf}} \quad (7)$$

$$\mathbf{S} = \mathbf{S}^{(1)} + \mathbf{S}^{(2)} \qquad \mathbf{I}^{(l)} = \sum_{k=1}^{m} \mathbf{I}^{(lk)}$$

where

$$A_{zz} = A_{XX}\sin^2\theta\cos^2\phi + A_{YY}\sin^2\theta\sin^2\phi + A_{ZZ}\cos^2\theta + A_{XY}\sin^2\theta\sin(2\phi) + A_{XZ}\sin(2\theta)\cos\phi + A_{ZY}\sin(2\theta)\sin\phi \quad (8)$$

and g_{zz}, μ_B, B_z, S, J, D_{zz}, and $I^{(l)}$ are the z component of the g tensor (defined analogous to eq 8), the Bohr magneton, the static magnetic field, the total electron spin operator, the electron–electron exchange parameter, the z component of the zero-field-splitting tensor (see eq 8), and the nuclear spin operator of the equivalent nuclei, respectively. Since pseudo- and nonsecular terms, $\mathcal{H}_{\text{p-sec}}$ and $\mathcal{H}_{\text{n-sec}}$, make only a slight correction to the line shape of rigid biradicals, we will ignore their effect[2] and approximate the eigenfunctions by simple products of the electron triplet and singlet functions

$$|1\rangle = |1,1\rangle$$
$$|2\rangle = |1,0\rangle$$
$$|3\rangle = |1,-1\rangle$$
$$|4\rangle = |0,0\rangle \quad (9)$$

and the nuclear spin functions $|M_1M_2\rangle$. Evaluating the density matrix equation of motion (eq 2) in this basis gives $N_\theta N_\phi$ coupled differential equations for each transition:

$$\dot{\rho}_{(ijM_1M_2)AB} = \rho_{(ijM_1M_2)AB}[i\omega_{(ijM_1M_2)AB} - 1/(T_2^0)_{(ij)AB} - k_{AA+1BB} - k_{AA-1BB} - k_{AABB+1} - k_{AABB-1}] + \rho_{(ijM_1M_2)A-1B}k_{A-1ABB} + \rho_{(ijM_1M_2)A+1B}k_{A+1ABB} + \rho_{(ijM_1M_2)AB-1}k_{AAB-1B} + \rho_{(ijM_1M_2)AB+1}k_{AAB+1B} + iK_{ij}[\rho_{(iiM_1M_2)AB} - \rho_{(jjM_1M_2)AB}]\exp(i\omega t) \quad (10)$$

where

$$\omega_{(ijM_1M_2)AB} = (1/\hbar)[\epsilon_{(jM_1M_2)AB} - \epsilon_{(iM_1M_2)AB}]$$

$$\epsilon_{1,M_1M_2} = g_{zz}\mu_B B_z + \tfrac{1}{4}J + \tfrac{1}{2}D_{zz} + \tfrac{1}{2}A_{zz}(M_1 + M_2)$$

$$\epsilon_{2,M_1M_2} = \tfrac{1}{4}J - D_{zz}$$

$$\epsilon_{3,M_1M_2} = -g_{zz}\mu_B B_z + \tfrac{1}{4}J + \tfrac{1}{2}D_{zz} - \tfrac{1}{2}A_{zz}(M_1 + M_2)$$

$$\epsilon_{4,M_1M_2} = -\tfrac{3}{4}J \quad (11)$$

$1/(T_2^0)_{(ij)AB}$ is a residual line width, and K_{ij} is a constant. For a weak microwave field we can take a steady-state solution of eq 10 without solving for the actual diagonal elements of the spin density matrix. To proceed, we replace all $\rho_{(iiM_1M_2)AB}$ by their thermal equilibrium values, introduce

$$\rho_{(ijM_1M_2)AB} = \sigma_{(ijM_1M_2)AB}\exp(i\omega t) \quad (12)$$

and separate the exponential. In the steady state (slow passage)

$$\dot{\sigma}_{(ijM_1M_2)AB} = 0 \quad (13)$$

and $N_\theta N_\phi$ coupled linear algebraic equations with $N_\theta N_\phi$ unknowns result. They are efficiently solved by employing the methods developed by Gordon & Messenger (1972). Summing up all contributions according to eq 1 finally gives the total line shape

$$L(\omega) = \text{Im}[\sum_{A,B}\sum_{M_1,M_2} F_{M_1M_2}(\sqrt{2}\sigma_{(21M_1M_2)AB} + \sqrt{2}\sigma_{(32M_1M_2)AB})] \quad (14)$$

where $F_{M_1M_2}$ accounts for the degeneracy of a particular transition. In the following section the theory will be applied to the analysis of temperature- and angular-dependent ESR spectra of BVL spin probes in oriented multibilayers of DMPC.

[2] Since rigid biradicals exhibit large zero-field splittings, pseudo-secular contributions are of minor importance and may be ignored.

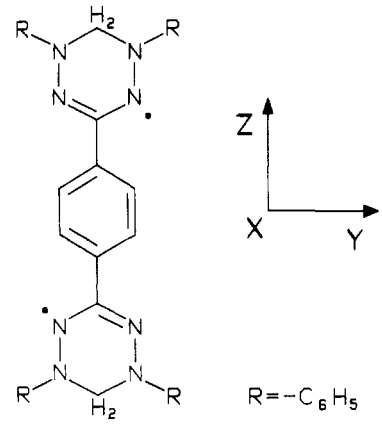

FIGURE 2: The structure of the BVL spin probe together with a molecular coordinate system, which diagonalizes the order and rotational diffusion tensor.

Materials and Methods

Materials. The synthesis of the BVL spin probe is described elsewhere (Kuhn et al., 1966). Figure 2 shows the structure of the biradical together with a molecular coordinate system, which diagonalizes the order and rotational diffusion tensor. DMPC was purchased from Fluka, Buchs, Switzerland, and the purity was checked by thin-layer chromatography. A solvent mixture containing 75% dichloromethane and 25% methanol (v/v) was used to dissolve both the lipid and the spin probe. The solvents were distilled from KOH pellets under nitrogen atmosphere. Dichloromethane was then water saturated. All solutions were prepared immediately before use. The biradical concentration was 0.15 mM, while the lipid concentration was 0.15 M.

Sample Preparation. Typically 35 μL of the above solution, corresponding to 5.25 nmol of spin probe and 5.25 μmol or 3.55 mg of lipid, was uniformly distributed on the bottom of an open quartz flat cell by means of a glass micropipet. The organic solvents were removed by first warming the sample cell on a water bath (60 °C, 1 min) and then placing it under vacuum (0.1 torr, 25 °C) for 15 min. The sample cell was then immersed into a water-saturated atmosphere (60 °C, 1 min) and finally closed with a tightly fitting cover. The amount of water which commonly condensed onto the sample was 15 mg. The above procedure yielded macroscopically oriented bilayer samples of high reproducibility. The quality of the samples was checked by recording the ESR spectra before and after each experiment under the same conditions (30 °C, $\rho = 0°$). It seems that angular-dependent ESR spectra are even more sensitive criteria for macroscopic orientation than optical birefringence (Powers & Clark, 1975).

ESR Measurements. The ESR measurements were performed on a Varian E-9 X-band spectrometer ($\omega = 5.8 \times 10^{10}$ s^{-1}), using 100-kHz field modulation. Orientation of the flat sample cell in the laboratory frame was achieved with a

Table I: Constant Parameters Used in the Calculation of the ESR Spectra of the BVL Spin Probes

nitrogen hyperfine tensor[a]	zero-field splitting tensor[a]	angular dependent residual line widths[b]
A_{XX}, 13.1 G	D_{XX}, ∓14.7 G	A_{21}', 2.0 G
A_{YY}, 2.3 G	D_{YY}, ∓14.7 G	X_{21}', 2.0 G
A_{ZZ}, 2.3 G	D_{ZZ}, ±29.4 G	A_{32}', 2.0 G
A_0[c], 5.9 G	g_0[d], 2.0033	X_{32}', 2.0 G

[a] Diagonal in X, Y, and Z (see Figure 2). [b] $(1/T_2^0)_{(ij)AB} = A_{ij}' + X_{ij}' \sin^2 \theta_A$. [c] Isotropic hyperfine coupling constant. [d] Isotropic g factor (g tensor anisotropy has been neglected).

home-built goniometer. The spectrometer was interfaced with a Hewlett-Packard 9845A computer, where the experimental spectra could be stored or transferred to a Univac 1100/80 computer. The scan range of the spectrometer was checked with an AEG nuclear magnetic resonance (NMR) gauss meter. The temperature of the sample was controlled by a home-built variable temperature control unit and was stable to ±0.2 °C.

Spectral Analysis. A Fortran program was employed to analyze the experimental spectra. The program TRISUPRO calculates ESR line shapes of rigid biradicals undergoing fast, intermediate, and slow molecular reorientation. A typical running time for one spectrum of the BVL biradical on the Univac 1100/80 is 180 s ($N_\theta N_\phi$ = 200). The calculated spectra were plotted on a Hewlett-Packard 9872A plotter. Table I summarizes the constant parameters used in the calculations. They were obtained from an analysis of the fast-rotational and rigid-limit spectra. Note that the angular-dependent residual line widths include the effect of proton hyperfine interactions, omitted in the spin Hamiltonian.

In order to reduce the number of adjustable parameters, we assume that the order tensor of the BVL biradical is axially symmetric along **Z**. This assumption is justified by the overall shape of the radical (see Figure 2), which is also expected to exhibit axially symmetric rotational diffusion about the Z axis. Using the appropriate expression (Shimizu, 1962), a theoretical anisotropy ratio $\tau_\perp/\tau_\parallel$ can be estimated from the dimensions of the molecule. For the BVL biradical we predict $\tau_\perp/\tau_\parallel$ = 2. Simulated experimental spectra with values $1 \leq \tau_\perp/\tau_\parallel \leq 10$ showed very little difference in the corresponding line shapes, which effectively depend only on $\tau_\perp$. We therefore characterize the ESR spectra by the correlation time $\tau_\perp$, assuming a constant ratio of $\tau_\perp/\tau_\parallel$ = 2.

Closer inspection of the experimental spectra revealed a superposition of spectra from BVL spin probes in two different environments. Thus two sets of simulation parameters had to be determined, employing the following procedure. Each experimental spectrum at $\rho = 0°$ was characterized, when possible, by two pairs of lines, corresponding to the different environments. From the separation and widths of these lines, first estimates for the rotational correlation times and orientational distributions were obtained. The values served as start parameters in the computer simulation of a set of seven angular-dependent spectra (15° interval) at any given temperature. An iterative fit of experimental and simulated line shapes finally provided reliable values for all spectral parameters, including the mole fractions of the spin probes in both environments.

Results

Typical ESR spectra of the BVL spin probes, incorporated into oriented DMPC multibilayers, are shown in Figures 3–5.

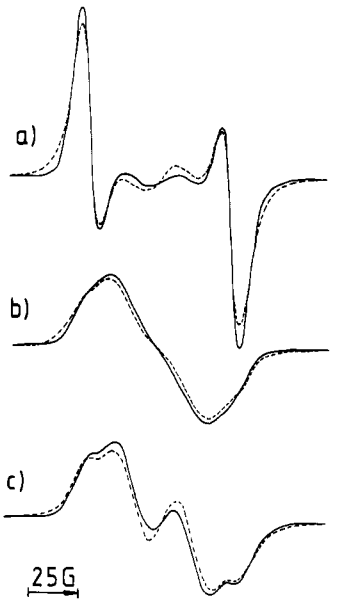

FIGURE 3: Experimental (—) and simulated (---) ESR spectra of the BVL spin probes in oriented multibilayers of DMPC at T = 25 °C and three different angles ρ between glass plate normal and magnetic field. The simulations were obtained with the parameters of Tables I and II and (a) $\rho = 0°$, (b) $\rho = 45°$, and (c) $\rho = 90°$. Note that all spectra are normalized to the same total intensity.

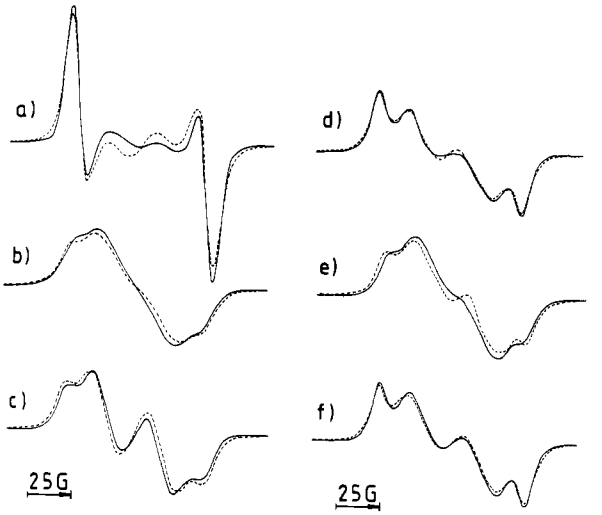

FIGURE 4: Experimental (—) and simulated (---) ESR spectra of the BVL spin probes in oriented multibilayers of DMPC at T = 17 °C and three different angles ρ between glass plate normal and magnetic field. The observed line shapes depend upon the sample history. The spectra a–c were taken at descending temperature whereas the spectra d–f were taken at ascending temperature after incubating at $T \sim 2$ °C. The simulations were obtained with the parameters of Tables I and II and (a) $\rho = 0°$, (b) $\rho = 45°$, (c) $\rho = 90°$, (d) $\rho = 0°$, (e) $\rho = 45°$, and (f) $\rho = 90°$. Note that all spectra are normalized to the same total intensity.

They refer to three temperatures and three orientations of glass plate and magnetic field. Drastic spectral changes are observed. In the temperature range below 23 °C the line shapes depend upon the sample history. Spectra for samples taken at descending temperature are different from those taken at ascending temperature when the samples have been incubated at 2 °C for about 10 min.

Calculated spectra were fitted to the experimental spectra by applying the procedure outlined above. The dotted lines in Figures 3–5 represent best fit simulations. They agree favorably with their experimental counterparts. Note that a combination of two sets of simulation parameters for spin probes in different environments was necessary to account for

Table II: Optimized Parameters Used in the Simulation of the ESR Spectra of the BVL Spin Probes Incorporated into Oriented Bilayers of DMPC[a]

	site I					site II				
	director distribution[b]		orientation parameter[c]	rotational correl. time[d] $\tau_\perp$	mole	director distribution[b]		orientation parameter[c]	rotational correl. time[d] $\tau_\perp$	mole
T (°C)	δ_{min}	δ_{max}	C	(ns)	fraction[e] x	δ_{min}	δ_{max}	C	(ns)	fraction[e] x
50	0	0	3.25	2.0	0.60	0	0	−1.00	5.5	0.40
47	0	0	3.40	2.3	0.60	0	0	−1.10	6.5	0.40
44	0	0	3.50	2.7	0.60	0	0	−1.20	8.0	0.40
41	0	0	3.65	3.0	0.60	0	0	−1.25	9.0	0.40
38	0	0	3.90	4.1	0.60	0	0	−1.35	11	0.40
34.5	0	0	3.95	4.9	0.60	0	0	−1.45	15	0.40
31	0	0	4.10	6.2	0.60	0	0	−1.55	17	0.40
28	0	0	4.30	7.8	0.60	0	0	−1.60	21	0.40
25	0	0	4.55	10	0.60	0	0	−1.70	25	0.40
23	0	17	9.2	36	0.60 (0.11)	0	17	−1.95	45	0.40 (0.89)
21	0	17	10.5	43	0.60 (0.11)	0	17	−1.95	53	0.40 (0.89)
19	0	18	11.2	55	0.60 (0.11)	0	18	−2.00	68	0.40 (0.89)
17	0	18	12.2	68	0.60 (0.11)	0	18	−2.05	86	0.40 (0.89)
15	0	19	13.3	84	0.60 (0.11)	0	19	−2.10	110	0.40 (0.89)
13	0 (22)	20 (22)	14.5	110	0.60 (0.08)	0 (0)	20 (0)	−2.15	140	0.40 (0.92)
11	0 (22)	20 (22)	16.0	135	0.60 (0.08)	0 (0)	20 (0)	−2.20	200	0.40 (0.92)
9	0 (23)	21 (23)	17.0	170	0.60 (0.08)	0 (0)	21 (0)	−2.25	270	0.40 (0.92)
7	0 (23)	21 (23)	17.5	210	0.60 (0.08)	0 (0)	21 (0)	−2.30	350	0.40 (0.92)
5	0 (23)	22 (23)	18.0	260	0.60 (0.08)	0 (0)	22 (0)	−2.30	420	0.40 (0.92)
3	0 (24)	22 (24)	18.5	340	0.60 (0.08)	0 (0)	22 (0)	−2.35	550	0.40 (0.92)
1	0 (24)	22 (24)	18.5	450	0.60 (0.08)	0 (0)	22 (0)	−2.35	650	0.40 (0.92)

[a] The numbers in parentheses result from simulations of spectra taken at ascending temperature. [b] See eq 6. The uncertainty in fixed tilt angles ($\delta_{min} = \delta_{max}$) is <2°. [c] See eq 4. [d] $\tau_\perp$ refers to reorientation of the symmetry axis of the rotational diffusion tensor (see Figure 2). [e] Mole fraction of the spin probes. The uncertainty in x (<0.03) is of the same magnitude as the temperature dependence of x.

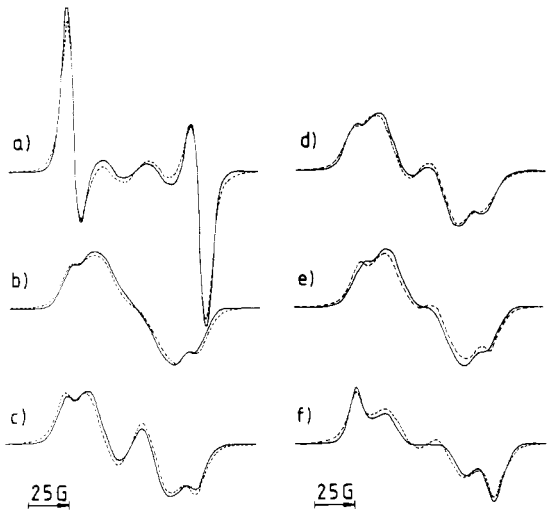

FIGURE 5: Experimental (—) and simulated (---) ESR spectra of the BVL spin probes in oriented multibilayers of DMPC at T = 5 °C and three different angles ρ between glass plate normal and magnetic field. The observed line shapes depend upon the sample history. The spectra a–c were taken at descending temperature whereas the spectra d–f were taken at ascending temperature after incubating at $T \sim 2$ °C. The simulations were obtained with the parameters of Tables I and II and (a) $\rho = 0°$, (b) $\rho = 45°$, (c) $\rho = 90°$, (d) $\rho = 0°$, (e) $\rho = 45°$, and (f) $\rho = 90°$. Note that all spectra are normalized to the same total intensity.

the observed line shapes. The agreement between experimental and calculated spectra could be improved by adding spectra, accounting for 10–12% of unoriented material. This relatively low amount supports the employed technique of sample preparation.

Table II summarizes the parameters, obtained from the simulations, i.e., the parameters of the director distribution δ_{min} and δ_{max} (see eq 6), the parameter of orientation C (see eq 4), the rotational correlation time $\tau_\perp$, and the mole fraction x of the spin probe in a particular site (environment). The numbers in parentheses refer to simulations of spectra, taken at ascending temperature. In the following we would like to describe the results in more detail, treating both sites separately.

Site I. In the liquid-crystalline phase the director orients parallel to the bilayer normal. For the intermediate phase two different kinds of spectra are observed, depending on the direction of the temperature scan. With decreasing temperature the mole fraction x = 0.60 does not change at the main transition; only the director axis suddenly shows a random distribution between 0° and 17°, which becomes even broader when the temperature is lowered. No change in x and the director distribution is found at the pretransition temperature, due to hysteresis effects (Luna & McConnell, 1977). The changes only occur ~10 °C below the normal pretransition temperature. Then, however, x changes drastically from 0.60 to 0.08, and the distribution of the director becomes very narrow again, showing a fixed tilt angle of δ = 24° with respect to the bilayer normal. When the sample is reheated, changes in x and the director orientation are found at the normal pretransition temperature of 13.5 °C. The change in x is only small this time, so that in the intermediate phase actually two different populations with different x exist.

The parameter C, which characterizes the local order of the spin probes, is always positive, indicating that the preferential orientation is parallel to the director. One sees, that the rotational correlation times of the spin probes increase with decreasing temperature. A logarithmic plot of $\tau_\perp$ vs. $1/T$ gives straight lines within the phases and a jump at the main transition. The activation energies evaluated from this plot are E_{rot} = 10.8 kcal/mol in the liquid-crystalline phase and E_{rot} = 18.4 kcal/mol in the gel phase (see Table III).

Site II. In the liquid-crystalline and intermediate phase spin probes occupying site II reflect the same director distribution as those in site I. However, below the pretransition (at as-

Table III: Dynamic Parameters Characterizing the Different Phases of DMPC Bilayers

	site I[a]		site II[b]	
phase	rotational activation energy[c] E_{rot} (kcal/mol)	activation energy of the viscous flow E_{visc} (kcal/mol)	rotational activation energy[c] E_{rot} (kcal/mol)	activation energy of the viscous flow E_{visc} (kcal/mol)
L_α	10.8	10.2	10.2	9.6
$P_{\beta'}$	18.4	17.7	19.2	18.5
$L_{\beta'}$	18.4	17.7	19.2	18.5

[a] Site I is associated with the hydrocarbon chain region. [b] Site II denotes the bilayer–water interface. [c] E_{rot} refers to reorientation of the symmetry axis of the BVL spin probes (see Figure 2). Considerably smaller values for the gel phase, previously determined on the basis of Redfield's theory, are incorrect (see Discussion).

cending temperature), a fixed tilt angle of 0° is found.

The parameters of local orientation are always negative, indicating that biradicals in this site orient perpendicular to the director axis. The rotational correlation times for probes in site II are significantly longer, showing only a slight discontinuity in the logarithmic plot. The rotational activation energies, however, fully compare with those in site I (see Table III).

Discussion

The thermotropic phase behavior of DMPC has been studied by numerous techniques which show that at maximum hydration DMPC (≥25% water) undergoes two transitions, a main transition around 24 °C (T_c^2), arising from the "melting" of the hydrocarbon chains, and a so-called pretransition between two different gel phases at 13.5 °C (T_c^1) [for a review, see Lee (1977)]. X-ray investigations have shown that the hydrocarbon chains in the $L_{\beta'}$ phase below T_c^1 are fully extended, tilted with respect to the bilayer normal, and packed in a quasihexagonal lattice (Tardieu et al., 1973; Ranck et al., 1974; Janiak et al., 1976, 1979). In the L_α phase above T_c^2 the chains are fluidlike with an increased number of gauche conformations, and there is no tilt of the chains. The $P_{\beta'}$ structure between T_c^1 and T_c^2 consists of stacked lamellae distorted by a periodic ripple in the plane of the lamellae (Tardieu et al., 1973; Ranck et al., 1974; Janiak et al., 1976, 1979). While there is no question that the bilayer surface is indeed rippled—this can also be observed by freeze–fracture electron microscopy (Verkleij et al., 1972; Luna & McConnell, 1977; Gebhardt et al., 1977)—no conclusive results about the orientation of the hydrocarbon chains with respect to the macroscopic plane of the bilayers could be obtained. A recent detailed X-ray analysis by Janiak et al. (1979) could show that a peristaltic structure as discussed for egg phosphatidylcholine (Ranck et al., 1974) could not be fitted to the observed diffraction pattern. Janiak et al. (1979) obtained a reasonable good fit between experimental and calculated diffraction patterns, assuming that the chains in the rippled phase are tilted. However, several other models have been proposed for the $P_{\beta'}$ phase. Larsson (1977) suggested folded bilayers whereas Gebhardt et al. (1977) interpreted the ripple structure in terms of spontaneous local curvature of the monolayers. Brady & Fein (1977) analyzed the wide-angle diffraction pattern and concluded that a change in tilt angle takes place at the pretransition. This was suggested earlier by Rand et al. (1975). Unfortunately, however, all X-ray data obtained are essentially not precise enough to distinguish between the different models suggested for the $P_{\beta'}$ phase (Janiak et al., 1979).

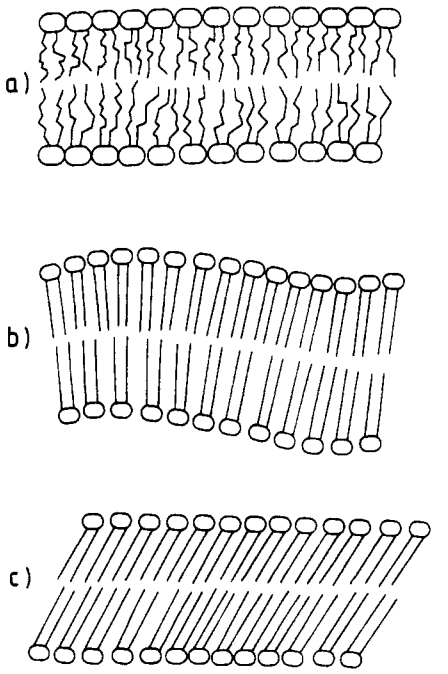

FIGURE 6: Schematic diagram of bilayer structures characterizing the (a) liquid crystalline, (b) ripple, and (c) gel phases of fully hydrated phosphatidylcholines. Circles represent head groups, straight lines fully extended hydrocarbon chains, and wiggly lines melted hydrocarbon chains.

The use of biradical spin probes in macroscopically oriented bilayers offers the chance to determine the chain tilt unambiguously. The preferential orientation of probe molecules in site I indicates that they are located in the hydrocarbon chain region. Consequently the director, experienced by these probes, can be identified with the average chain orientation. Inspection of Table II reveals that in the $L_{\beta'}$ phase the chains are uniformly tilted with respect to the bilayer normal (see Figure 6c). The observed tilt angle of $\delta = 22$–$24°$ agrees with X-ray data (Tardieu et al., 1973; Janiak et al., 1976, 1979). In accordance with other observations we find no tilt for the L_α phase (see Figure 6a). A finite tilt angle, as obtained with nitroxide spin probes (McConnell & McFarland, 1972), may result from the noncolinearity of hyperfine and order tensor. Note, that in the BVL probes zero-field splitting and order tensor strictly coincide.

Our results for the chain orientation in the $P_{\beta'}$ phase (random distribution of tilt angles between 0° and 19°) cannot be reconciled with the model suggested by Janiak et al. (1976, 1979) and Doniach (1979) nor with the model of folded bilayers proposed by Larsson (1977). In these models the chains always have the same orientation with respect to the tangent plane of the ripple surface. Our results rather favor a model where the chains orient perpendicular to the local bilayer surface (see Figure 6b). Because the bilayers display a periodic ripple, the orientation of the chains varies with respect to the glass plate normal. From our δ_{max} values we can in fact determine the amplitude to wavelength ratio assuming sinusoidal ripples. At 23 °C this ratio is 0.049 and increases to 0.055 at 15 °C. Taking an amplitude value of 7.5 Å (Janiak et al., 1979), we calculate ripple periods of 150 (23 °C) and 140 Å (15 °C). These values are in excellent agreement with data obtained by Copeland & McConnell (1980), using freeze–fracture electron microscopy.

Probe molecules in site II show negative orientation parameters and no director tilt for the L_α and $L_{\beta'}$ phase, indicating a preferential orientation of the long axes parallel to the bilayer plane. Because of the polar character, these probes

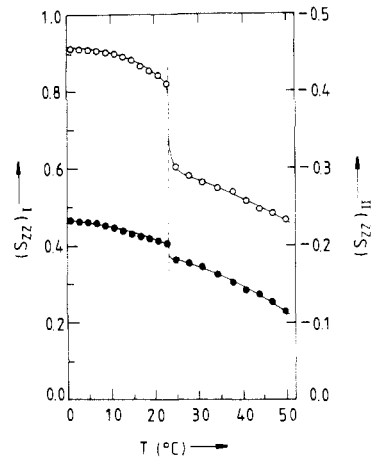

FIGURE 7: Temperature dependence of the order parameters S_{ZZ} of the BVL spin probes occupying two different sites of DMPC bilayers. Open circles (left ordinate scale) denote site I (hydrocarbon chain region), full circles (right ordinate scale) denote site II (bilayer–water interface), and the dashed line indicates the main transition.

are most likely located at the bilayer–water interface and reflect the orientation of the bilayer surface. In the $P_{\beta'}$ phase the bilayers are rippled. This should lead to a variation of the director tilt, which is indeed observed for probes in site II likewise. The spectral simulations show that all biradicals, independent of their location, experience a broad director distribution in the $P_{\beta'}$ phase (see Table II). We therefore conclude that in this phase the bilayer surface is rippled and the lipid chains are always perpendicular to the local bilayer surface (see Figure 6b). This model agrees with the symmetry of the defects found by Gebhardt et al. (1977), using freeze–fracture electron microscopy.

Interestingly, the mole fraction x changes at the $L_{\beta'} \rightarrow P_{\beta'}$ transition, indicating a slight difference in the hydrocarbon chain packing of the two gel phases. Apparently, in the $P_{\beta'}$ phase more spin probes can be accommodated between the chains. Similar results have been obtained previously with other probe molecules (Lee, 1975; Luna & McConnell, 1977). The above observations can be reconciled with our model for the $P_{\beta'}$ phase (see Figure 6b), which is slightly more disordered than the $L_{\beta'}$ phase.

As mentioned earlier, we find a large hysteresis of ~10 °C for the pretransition. Moreover, the mole fraction x does not change at the $L_\alpha \rightarrow P_{\beta'}$ main transition. A change in x only occurs ~20 °C below, when the $P_{\beta'} \rightarrow L_{\beta'}$ pretransition takes place. Then most of the spin probes are expelled from the bilayer interior. At ascending temperature, however, a large change of x occurs at the main transition. So, apart from the hysteresis of the pretransition, we observe another hysteresis for the probe distribution, which is coupled to the pretransition. The phenomenon is not observed with other probe molecules but seems to be characteristic for this biradical.[3]

We now discuss the local order of the biradical probes in terms of the familiar order parameter S_{ZZ}, characterizing the average orientation of the molecular Z axes (see Figure 2) with respect to the director (Saupe, 1964). S_{ZZ} is readily calculated from the orientation parameter C by evaluating the integrals:

$$S_{ZZ} = \tfrac{1}{2}N_3 \int_0^\pi (3\cos^2\beta - 1)\exp(C\cos^2\beta)\sin\beta\, d\beta$$

$$1/N_3 = \int_0^\pi \exp(C\cos^2\beta)\sin\beta\, d\beta \qquad (15)$$

[3] A reviewer pointed out that hysteresis in the mole fraction x occurs for other probes, but the effect has not yet been published.

Figure 7 shows the temperature dependence of the order parameters for the BVL biradicals, occupying two different sites of DMPC bilayers. Open circles (left ordinate scale) denote site I, while full circles (right ordinate scale) refer to site II. One sees that both types of parameters are sensitive to the phospholipid state. The order parameters for probes in site I (hydrocarbon chain region) jump at the main transition from $S_{ZZ} = 0.60$ to $S_{ZZ} = 0.82$. The abrupt rise of S_{ZZ} reflects the increase of local chain order in the $P_{\beta'}$ phase. Interestingly, the order parameters for probes in site II (bilayer–water interface) also exhibit a discontinuity at the main transition, indicating that the bilayer–water interface is affected by the state of the hydrocarbon chains.

In comparing the BVL order parameters with lipid order parameters as determined by ^2H NMR (Seelig & Seelig, 1974; Davis, 1979), one major difference has to be considered. ^2H NMR measures the order parameter of an individual segment along the chain whereas ESR measures the order parameter of the probe between the chains. Since the BVL biradical is ~16 Å long, it will reflect the order parameter of the entire chain. In view of this difference, only qualitative agreement between BVL and lipid order parameters can be expected and is indeed observed.

Finally we wish to discuss the molecular dynamics of the BVL spin probes in the DMPC bilayers. Inspection of Table II shows that the rotational correlation times range from $\tau_\perp = 2$ ns to $\tau_\perp = 650$ ns, implying that a fast-rotational lineshape theory is inadequate, since the condition

$$\tau_\perp \ll \hbar/|\tfrac{9}{4}D_{ZZ}| \qquad (16)$$

is no longer fulfilled. Similar is true for many nitroxide spin probes employed in lipids and membranes. Thus, most of the rotational correlation times, determined on the basis of Redfield's theory (Redfield, 1965), have at best qualitative significance and at worst lead to erroneous indications of phase transitions. This has been shown by spin probe studies, employing a slow-motional theory similar to that used in this paper (Cannon et al., 1975; Rao et al., 1977; Mason & Polnaszek, 1978; Meirovitch & Freed, 1980a,b).

So far, little is known about the dynamics of spin probes in the gel phase. This is mainly due to the fact that conventional ESR spectra of nitroxide probes are insensitive to motions with rotational correlation times $\tau_\perp > 100$ ns. With BVL probes, however, correlation times up to $\tau_\perp = 5000$ ns can be detected. This particular sensitivity of the BVL biradicals results from the anisotropy of the zero-field splitting, not available in monoradicals.

It was recently shown that the sensitivity of nitroxide spin probes can be extended to slower motions by saturation transfer electron spin resonance (STESR) spectroscopy (Hyde & Dalton, 1979). However, this method has mainly been applied to systems with isotopic molecular reorientation, since a satisfactory theoretical treatment of anisotropic motion is only lately available (Robinson & Dalton, 1980). First qualitative STESR studies of spin probes in model membranes indicate the onset of rapid long axis rotation at the pretransition (Marsh, 1980; Delmelle et al., 1980). We were unable to detect this motion, possibly because the ESR spectra of the BVL probes are rather insensitive to reorientation about the Z axis (see Spectral Analysis).

The rotational correlation times $\tau_\perp$ of the spin probes are related to the viscosity η of the surrounding matrix by a modified Debye equation

$$\tau_\perp = 4r_{e\perp}{}^3\pi\eta/(3kT) \qquad (17)$$

where $r_{e\perp}$ is an effective rotation radius, depending upon the

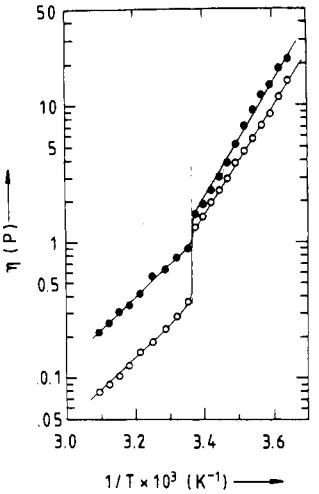

FIGURE 8: Arrhenius plot of viscosity η of DMPC bilayers. Open circles denote the hydrocarbon chain region, full circles denote the bilayer–water interface, and the dashed line indicates the main transition.

geometry of the probe and the nature of the rotor–matrix interactions. In favorable cases $r_{e\perp}$ can be determined from ESR studies of the spin probe in a comparable matrix of known viscosity. A plot of $\tau_\perp$ vs. η/T for the BVL probes in glyceryl trioleate is linear over the whole temperature range investigated, yielding an effective rotational radius of $r_{e\perp} = 6.4$ Å. We have taken this value to estimate the viscosity of the DMPC bilayers according to eq 17.

Strictly there are several independent viscosity coefficents for a bilayer membrane. The coefficient η used in this paper represents an average, characterizing a particular region (site) of the bilayer. In Figure 8 log η is plotted as a function of $1/T$. Open circles denote the hydrocarbon chain region, while full circles refer to the bilayer–water interface. The discontinuities observed correspond to the main phase transition. Above and below T_c[2] the plots are linear. From the slopes of the straight lines activation energies of the viscous flow have been determined. The values for E_{visc} differ, increasing from ~10 kcal/mol in the liquid-crystalline phase to ~18 kcal/mol in the gel phase[4] (see Table III).

The results are at variance with microviscosities determined from the steady-state fluorescence polarization (Cogan et al., 1973; Lentz et al., 1976). However, the standard procedure for the evaluation of microviscosities ignored the fact that the fluorescent probes are in an anisotropic environment. Recent studies (Heyn, 1979; Jähnig, 1979) have shown that consideration of the partial alignment of the probes may significantly reduce the microviscosity values, which indeed are by a factor of 2–5 larger than the viscosities of this paper. One can show that the error made by the neglect of a finite order parameter S_{zz} is proportional to S_{zz}^2 (Heyn, 1979). Thus the drastic change of the previously published microviscosities at the main transition is an artifact, resulting from the jump of the order parameter (see Figure 7). The relatively small change of η found in this study may be of significance for the function of biological membranes, where liquid-crystalline and gel phase lipids simultaneously exist.

Acknowledgments

It is a pleasure to thank Professors T. Ackermann and H. Zimmerman for their advice and continuous support. We are also indebted to T. Berthold for excellent technical assistance. The numerical calculations were carried out on a Univac 1100/80 at the computer center of the University of Freiburg.

[4] The smaller values for E_{visc}, given in a preliminary communication (Kothe et al., 1978), have been determined from ESR spectra of BVL probes in unoriented bilayers (liposomes) of DMPC.

References

Brady, G. W., & Fein, D. B. (1977) *Biochim. Biophys. Acta 464*, 249.

Cannon, B., Polnaszek, C. F., Butler, K. W., Eriksson, L. E. G., & Smith, I. C. P. (1975) *Arch. Biochem. Biophys. 167*, 505.

Cogan, U., Shinitzky, M., Weber, G., & Nishida, T. (1973) *Biochemistry 12*, 521.

Copeland, B. R., & McConnell, H. M. (1980) *Biochim. Biophys. Acta 599*, 95.

Cotter, M. A. (1977) *J. Chem. Phys. 66*, 1098.

Davis, J. H. (1979) *Biophys. J. 27*, 339.

Delmelle, M., Butler, K. W., & Smith, I. C. P. (1980) *Biochemistry 19*, 698.

Doniach, S. (1979) *J. Chem. Phys. 70*, 4587.

Forrester, R. A. (1980) in *Landoldt*-Börnstein, *New Series, Magnetic Properties of Free Radicals* (Fischer, H., & Hellwege, K.-H., Eds.) Vol. II/9d 2, pp 190–312, Springer-Verlag, West Berlin.

Freed, J. H., Bruno, G. V., & Polnaszek, C. F. (1971) *J. Phys. Chem. 75*, 3385.

Gebhardt, C., Gruler, H., & Sackmann, E. (1977) *Z. Naturforsch. C: Biosci. 32c*, 581.

Gordon, R. G., & Messenger, T. (1972) in *Electron Spin Relaxation in Liquids* (Muus, L. T., & Atkins, P. W., Eds.) pp 341–381, Plenum Press, New York.

Grell, E., Ed. (1981) *Membrane Spectroscopy*, Springer-Verlag, West Berlin.

Heyn, M. P. (1979) *FEBS Lett. 108*, 359.

Hyde, J. S., & Dalton, L. R. (1979) in *Spin Labeling: Theory and Applications* (Berliner, L. J., Ed.) Vol. II, pp 1–70, Academic Press, New York.

Jähnig, F. (1979) *Proc. Natl. Acad. Sci. U.S.A. 76*, 6361.

Janiak, M. J., Small, D. M., & Shipley, G. G. (1976) *Biochemistry 15*, 4575.

Janiak, M. J., Small, D. M., & Shipley, G. G. (1979) *J. Biol. Chem. 254*, 6068.

Keana, J. F. W., & Dinerstein, R. J. (1971) *J. Am. Chem. Soc. 93*, 2808.

Kothe, G. (1977) *Mol. Phys. 33*, 147.

Kothe, G., & Wilker, W. (1980) in *Landolt-Börnstein, New Series, Magnetic Properties of Free Radicals* (Fischer, H., & Hellwege, K.-H., Eds.) Vol. II/9d 2, pp 148–189, Springer-Verlag, West Berlin.

Kothe, G., Ohmes, E., Meier, P., & Blume, A. (1978) *Ber. Bunsenges. Phys. Chem. 82*, 916.

Kothe, G., Wassmer, K.-H., Naujok, A., Ohmes, E., Rieser, J., & Wallenfels, K. (1979) *J. Magn. Reson. 36*, 425.

Kubo, R. (1969) *Adv. Chem. Phys. 16*, 101.

Kuhn, R., Neugebauer, F. A., & Trischmann, H. (1966) *Monatsh. Chem. 97*, 525.

Larsson, K. (1977) *Chem. Phys. Lipids 20*, 225.

Lee, A. G. (1975) *Biochemistry 14*, 4397.

Lee, A. G. (1977) *Biochim. Biophys. Acta 472*, 237.

Lentz, B. R., Barenholz, Y., & Thompson, T. E. (1976) *Biochemistry 15*, 4521.

Luckhurst, G. R. (1976) in *Spin Labeling: Theory and Applications* (Berliner, L. J., Ed.) Vol. 1, pp 133–181, Academic Press, New York.

Luna, E. J., & McConnell, H. M. (1977) *Biochim. Biophys. Acta 466*, 381.

Maier, W., & Saupe, A. (1959) *Z. Naturforsch. A 14A*, 882.

Marsh, D. (1980) *Biochemistry 19*, 1632.

Mason, R. P., & Polnaszek, C. F. (1978) *Biochemistry 17*, 1758.
McConnell, H. M., & McFarland, B. G. (1972) *Ann. N.Y. Acad. Sci. 195*, 207.
Meirovitch, E., & Freed, J. H. (1980a) *J. Phys. Chem. 84*, 3281.
Meirovitch, E., & Freed, J. H. (1980b) *J. Phys. Chem. 84*, 3295.
Norris, J. R., & Weissman, S. I. (1969) *J. Phys. Chem. 73*, 3119.
Powers, L., & Clark, N. A. (1975) *Proc. Natl. Acad. Sci. U.S.A. 72*, 840.
Ranck, J. L., Mateu, L., Sadler, D. M., Tardieu, A., Gulik-Krzywicki, T., & Luzzati, V. (1974) *J. Mol. Biol. 85*, 249.
Rand, R. P., Chapman, D., & Larsson, K. (1975) *Biophys. J. 15*, 1117.
Rao, K. V. S., Polnaszek, C. F., & Freed, J. H. (1977) *J. Phys. Chem. 81*, 449.
Redfield, A. G. (1965) *Adv. Magn. Reson. 1*, 1.
Reitz, D. C., & Weissman, V. I. (1960) *Z. Chem. Phys. 33*, 700.
Robinson, H. B., & Dalton, L. R. (1980) *J. Chem. Phys. 72*, 1312.
Saupe, A. (1964) *Z. Naturforsch. A 19A*, 161.
Seelig, A., & Seelig, J. (1974) *Biochemistry 13*, 4839.
Shimizu, H. (1962) *J. Chem. Phys. 37*, 705.
Tardieu, A., Luzzati, V., & Reman, F. C. (1973) *J. Mol. Biol. 75*, 711.
Van, S. P., Birrell, G. P., & Griffith, O. H. (1974) *J. Magn. Reson. 15*, 444.
Verkleij, A. J., Ververgaert, P. H. J., van Deenen, L. L. M., & Elbers, P. F. (1972) *Biochim. Biophys. Acta 288*, 326.

Interaction of Tubulin with Single Ring Analogues of Colchicine†

Jose Manuel Andreu and Serge N. Timasheff*

ABSTRACT: Simple analogues of the tropolone and trimethoxyphenyl moieties of colchicine have been used as probes for the colchicine binding site of purified calf brain tubulin. [^{3}H]Tropolone methyl ether was found to bind to one site per tubulin molecule with an equilibrium constant of (2.2 ± 0.2) × 10^3 M^{-1} at 0 °C, with the interaction having $\Delta H°_{app}$ = −8.3 ± 1.0 kcal mol^{-1} and $\Delta S°_{app}$ = −15.2 ± 3.6 eu. The binding of tropolone methyl ether and colchicine was inhibited by each other. Both tropolone and its methyl ether inhibited tubulin polymerization into microtubules in vitro. *N*-[^{3}H]Acetylmescaline bound to tubulin with a $K \simeq 4 \times 10^2$ M^{-1} at 37 °C. This interaction was inhibited by colchicine and at lower temperatures was below the sensitivity of the measuring method employed. [^{14}C]Mescaline interacted with higher affinity site(s) not related to the colchicine site. Both mescaline and *N*-acetylmescaline inhibited partially the microtubule assembly at 10^{-3} M concentrations. No linkage was observed between the binding of tropolone methyl ether and *N*-acetylmescaline. The relatively weak interactions of both the two separate parts of colchicine can account quantitatively for the much tighter binding of the complete drug to tubulin within a proposed model which takes into account the entropic advantage of colchicine as a bifunctional ligand.

Colchicine and podophyllotoxin inhibit mitosis by interacting with the microtubule protein tubulin (Wilson & Bryan, 1974). These alkaloids have been used extensively for the inhibition of microtubule-mediated processes in vivo and have become important tools in the study of the mechanism of tubulin assembly into microtubules in vitro (Margolis & Wilson, 1977, 1978). In vitro, the assembly of pure tubulin into microtubules is known to conform thermodynamically to the Oosawa & Kasai (1971) model of nucleated helical polymerization (Lee & Timasheff, 1977). The actual kinetic pathway of microtubule assembly is probably much more complicated, but the final state is a steady state resulting from the incorporation and release of protomers at the ends of the microtubules. This can lead to an apparent movement of tubulin subunits from one end of the organelle to the other without changing its size, as described by the treadmilling mechanism of Margolis & Wilson (1978) (Karr & Purich, 1979; Bergen & Borisy, 1980). Colchicine and podophyllotoxin bind to soluble tubulin and inhibit microtubule assembly substoichiometrically, as incorporation of liganded protein at microtubule ends inhibits further polymer growth (Margolis & Wilson, 1977; Sternlicht & Ringel, 1979).

The interaction of colchicine with soluble tubulin is a complex and poorly understood phenomenon. The binding is slow and not easily reversed. The stoichiometry is close to one site per tubulin dimer. The binding site denatures rapidly, hampering equilibrium studies of the process (Wilson & Bryan, 1974). Nevertheless, different studies of the binding affinity of colchicine for brain tubulins of various origins, either purified or containing microtubule associated proteins, carried out by different techniques and under a variety of conditions (nature of buffer anions, presence of sucrose, Mg^{2+}, etc.) (Owellen et al., 1972; Wilson & Bryan, 1974; Bhattacharyya & Wolff, 1974; Sherline et al., 1975; Garland, 1978; Nunez et al., 1979) have given results not very different from each other. Indeed if the standard free energies of the binding reaction are averaged, the colchicine–tubulin interaction at pH 6.5–7.0, 37 °C, would have a $\Delta G°_{app}$ of −9.0 ± 0.2 kcal mol^{-1}. If, instead of equilibrium measurements, kinetic measurements are used to calculate the equilibrium constant, the numbers that come out give $\Delta G°_{app}$ = −10.3 ± 0.3 kcal mol^{-1}. This analysis strongly suggests that (i) the colchicine–tubulin interaction affinity is not significantly dependent on the origin of the brain tubulin, the small amounts of mi-

† From the Graduate Department of Biochemistry, Brandeis University, Waltham, Massachusetts 02254. *Received June 3, 1981.* This work is Publication No. 1387. This research was supported by Grants CA 16707 and GM 14603 from the National Institutes of Health, a fellowship from the U.S.A.–Spain Joint Committee for Scientific and Technological Cooperation (J.M.A.), and a Fogarty International Fellowship from the National Institutes of Health (J.M.A.). A preliminary report of this work has been presented elsewhere (Andreu & Timasheff, 1981a).

0006-2960/82/0421-0534$01.25/0